

Low-threshold, mid-infrared backward-wave parametric oscillator with periodically poled Rb:KTP ^{EP}

Cite as: APL Photonics 3, 071302 (2018); <https://doi.org/10.1063/1.5035493>
 Submitted: 16 April 2018 • Accepted: 29 May 2018 • Published Online: 20 June 2018

Riaan Stuart Coetzee, Andrius Zukauskas, Carlota Canalias, et al.

COLLECTIONS

^{EP} This paper was selected as an Editor's Pick



View Online



Export Citation



CrossMark

ARTICLES YOU MAY BE INTERESTED IN

PROPOSED BACKWARD WAVE OSCILLATION IN THE INFRARED

Applied Physics Letters 9, 114 (1966); <https://doi.org/10.1063/1.1754668>

Injection-seeded backward terahertz-wave parametric oscillator

APL Photonics 5, 061301 (2020); <https://doi.org/10.1063/5.0007306>

Quasi-phase matching waveguides on lithium niobate and KTP for nonlinear frequency conversion: A comparison

APL Photonics 6, 091102 (2021); <https://doi.org/10.1063/5.0060096>

AMERICAN ELEMENTS
THE ADVANCED MATERIALS MANUFACTURER

The Next Generation of Material Science Catalogs

yttrium iron garnet	glass/ceramic	beam splitters	fluxed quartz	additive manufacturing
zinc telluride	Bi-Si semiconductors	gallium nitride	epitaxial nanoparticles	organic materials
rare earths	carbon nanotubes	europium phosphates	photonic crystals	infrared dyes
optical crystal growth	ultra-high purity materials	transparent ceramics	CMOS	
calcium oxide polishing powders	oxide functionalized nanoparticles	emmet	nanodiamonds	
silicon nanoparticles	perovskites	SiC	graphene materials	nanofibers
MOCVD	beta boron borate		OLED lighting	solar energy
rare earth metals	quantum dots		spontaneous targets	Fiber optics
semiconductors	scintillation Ca:YAG		UV	deposition slugs
refractory metals	layer crystals		CVD precursors	photovoltaics
oxide	lithium niobate	indium wafers	metamaterials	boron-doped glass
aluminum nitride	MOFs	AuNPs	PERC	superconductors
chalcogenides	2D	SiP	indium tin oxide	AgCl
perovskite crystals	transparent ceramics		dielectric microresonators	optical lattice

Now Invent.

www.americanelements.com



Low-threshold, mid-infrared backward-wave parametric oscillator with periodically poled Rb:KTP

Riaan Stuart Coetzee,^a Andrius Zukauskas, Carlota Canalias,
and Valdas Pasiskevicius

*Department of Applied Physics, Royal Institute of Technology, Roslagstullsbacken 21,
10691 Stockholm, Sweden*

(Received 16 April 2018; accepted 29 May 2018; published online 20 June 2018)

We report on the development of a nanosecond mirrorless optical parametric oscillator (OPO) pumped at 1 μm . The gain medium of the OPO was periodically poled Rubidium-doped KTP with a grating period of $\Lambda = 509$ nm for the first order quasi-phase matching. For grating periods of this length, we demonstrate backward propagation of the signal field and forward propagation of the idler field. To the best of our knowledge, this is the first time such a counter-propagating geometry has been demonstrated in mirrorless OPOs. Pumping with a maximum energy of 6.48 mJ, the OPO yielded an overall conversion efficiency exceeding 53% with signal and idler energies of 1.96 mJ and 1.46 mJ, respectively. The generated signal and idler field spectra were measured to show narrowband linewidths on the order of 0.5 nm. We motivate that such a MOPO is ideal for seeding applications and discuss further improvements and work. © 2018 Author(s). All article content, except where otherwise noted, is licensed under a Creative Commons Attribution (CC BY) license (<http://creativecommons.org/licenses/by/4.0/>). <https://doi.org/10.1063/1.5035493>

I. INTRODUCTION

Backward-wave optical parametric oscillators¹ (BWOPOs) like their electronic counterparts which were proposed much earlier^{2,3} can sustain oscillations owing to a self-established positive feedback mechanism. In BWOPO, such a mechanism relies on three-wave mixing (TWM) between the counter-propagating signal and idler waves in the presence of a co-propagating pump beam. Such oscillators possess properties which are rather unusual for optical parametric oscillators (OPOs). First, owing to the fact that the oscillation is established by the distributed feedback and not by any external cavity, the pump intensity at the threshold will depend primarily on the length and nonlinearity of a nonlinear medium.^{1,4–6} Second, the parametric wave (signal or idler) which is generated in the opposite direction to that of the pump is inherently narrowband and largely insensitive to the pump frequency variation. The energy conservation then ensures that this variation is inherited by the complementary parametric wave generated in the forward direction.^{7–9} Third, the frequencies of the parametric waves generated in BWOPO are substantially less sensitive to the nonlinear crystal temperature and pump angle variations, as compared to the conventional OPOs.^{7,10} Such properties are conducive to achieve a narrowband precisely tunable near- and mid-infrared wavelength generation with scalable output energy in a simple and robust arrangement. This would be beneficial in a number of applications including sources of nonclassical light,¹¹ remote sensing and differential absorption LIDARs, and others, where seeded or doubly resonant OPOs are currently employed.^{12–14}

The BWOPO oscillation in near- and mid-infrared can be realized if momentum conservation in counter-propagating TWM is satisfied. With the available second-order nonlinear materials, this can be achieved only in quasi-phase matched (QPM) structures¹⁵ with sub- μm periodicity.

^arc@laserphysics.kth.se

So far, such structures have been demonstrated by employing periodic poling in KTiOPO_4 (KTP) isomorphs⁷ owing to its beneficial mm^2 crystalline structure and substantial anisotropy of the ferroelectric domain growth during the poling process. The first demonstrations of BWOPO required pump intensities substantially higher than 1 GW cm^{-2} which mandated pumping with picosecond pulses.^{7,8,10} It would be impractical to operate BWOPO using such structures within the nanosecond pulse regime due to competition from stimulated Raman scattering processes as well as close proximity to the optical damage threshold, even though the optical damage threshold in this material is rather high.^{16,17}

In this work, we show that improved structuring methods now allow the fabrication of periodically poled Rb-doped KTP (PPRKTP) structures with sub- μm periodicity, where the BWOPO thresholds are similar to those regularly obtained in low threshold nanosecond PPKTP OPO devices using the usual co-propagating TWM interaction. These advances allowed the reliable operation of BWOPO pumped by 10 ns Q-switched pulses, generating narrowband pulses with an output energy of 3.4 mJ with conversion efficiency exceeding 53%. Moreover, as we show here, such a performance can now be achieved in PPRKTP structures with the QPM periodicity as small as 509 nm.¹⁸

II. BWOPO PHASE MATCHING

BWOPO employs counter-propagating TWM, which has to satisfy the momentum conservation condition $k_p - K_g = \pm k_s \mp k_i$, where k_j ($j = p, s, i$) denote the wave vectors of the pump, signal, and idler, respectively, and $K_g = 2\pi/\Lambda$ is the wave vector of the QPM structure with periodicity Λ . Here we use the standard convention for the signal and idler frequencies $\omega_s \geq \omega_i$. The upper signs in the momentum conservation condition correspond to the case where the idler wave is generated in the opposite direction to the pump, while the lower signs—to the case where the signal is generated backwards. The calculated dependence of the signal wavelength on Λ in these two cases is shown in Fig. 1, for the pump wavelength of $1.064 \mu\text{m}$. Here we employed Sellmeier expansions for KTP18, which are suitable for RKTP with Rb concentrations below 1%, which is the doping concentration of the crystals used in this work.

As can be seen from Fig. 1, the signal at the wavelength of $1.85 \mu\text{m}$ can be generated in the direction parallel or antiparallel to the pump in PPRKTP structures with the period of 692 nm or 500 nm, respectively. So far, all demonstrations of the BWOPO employed longer periods, where the signal is generated parallel to the pump. However, in this geometry, the BWOPO has freedom to start cascaded oscillations where the signal of the first process plays the role of the pump.¹⁹ In some applications, this is not desirable as these cascaded oscillations would generate additional spectral

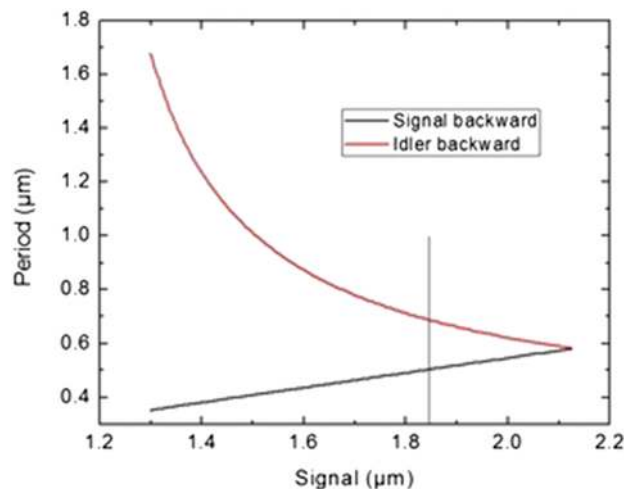


FIG. 1. Dependence of the BWOPO signal wavelength on the QPM period Λ in KTP for the $1.064 \mu\text{m}$ pump. Red line: signal generated in the direction of the pump; black line: signal generated in the opposite direction. The signal and idler are always collinear and counter-propagating. The vertical line marks the signal wavelength generated in this work.

lines and the efficiency of the first process will be limited. Such cascading does not occur in BWOPO with a backward-generated signal. This asymmetry stems from the BWOPO fundamental property that the frequency of the parametric wave generated in the opposite direction to the pump is mostly determined by the QPM grating and does not vary substantially when the frequency of the pump is changed. Then from momentum and energy conservation conditions, it directly follows that, in BWOPO with backward signal generation, the first cascaded process would require generation of an idler wave with a negative frequency. Obviously, this is unphysical and therefore cascading in such devices does not happen.

However, as evident from Fig. 1, achieving the BWOPO regime with the backward generated signal requires substantially shorter QPM periodicity. Specifically, for a given pump wavelength λ_p , the periodicity of the QPM structure must satisfy the inequality $\Lambda < 2\lambda_p/(2n_p + n_s - n_i)$, where n_j denotes the corresponding refractive indices. RKTp has so far proved to be the most suitable ferroelectric material for fabricating such sub- μm -periodicity structures over the volumes required for low-threshold, nanosecond, millijoule-level BWOPOs. Low Rb-doping ($\sim 0.3\%$) contributes in reducing the ionic conductivity of pure KTP by several orders of magnitude²⁰ without substantially modifying its linear and nonlinear properties. Moreover, the doping greatly reduces color-center accumulation effects, usually observed in undoped KTP under exposure by high-intensity light in the blue spectral region.²¹

III. EXPERIMENTAL SETUP AND RESULTS

For the BWOPO pumped at $1.064\ \mu\text{m}$ and generating a backward signal at $1.856\ \mu\text{m}$, we chose the PPRKTP periodicity of $509\ \text{nm}$. The fabrication process starts with interferometric UV-laser lithography together with liftoff in order to define an Al-surface mask. Then, a coercive field grating is created in the crystal by performing ion-exchange through the Al-mask. After that the metal is removed and periodic poling is achieved by applying $5\ \text{ms}$ long pulses of an electric field strength of $6.2\ \text{kV/mm}$. The periodic modulation of the coercive field in the volume close to the crystal surface is crucial since it alleviates the fringing-field problem associated with periodic metal electrodes.²³ The procedure is described in more detail in Refs. 19, 22, and 23. The fabricated crystal had a homogeneous poled volume of $7\ \text{mm} \times 3\ \text{mm} \times 1\ \text{mm}$ as measured along the crystal a , b , c axes, respectively.

Shown in Fig. 2 is the resulting domain structure revealed by chemical etching on (a) the patterned face and (b) the opposite face. Note that the inverted domains appear as light lines in (a), whereas they are dark lines in (b). The surfaces perpendicular to the crystal a -axis were polished to optical quality and left uncoated. Pumping and BWOPO oscillation were achieved along the a -axis of the crystal for waves polarized parallel to the polar c -axis, i.e., employing the d_{33} nonlinear coefficient. The experimental setup is shown in Fig. 3. The BWOPO was pumped by a Q-switched, injection-seeded,

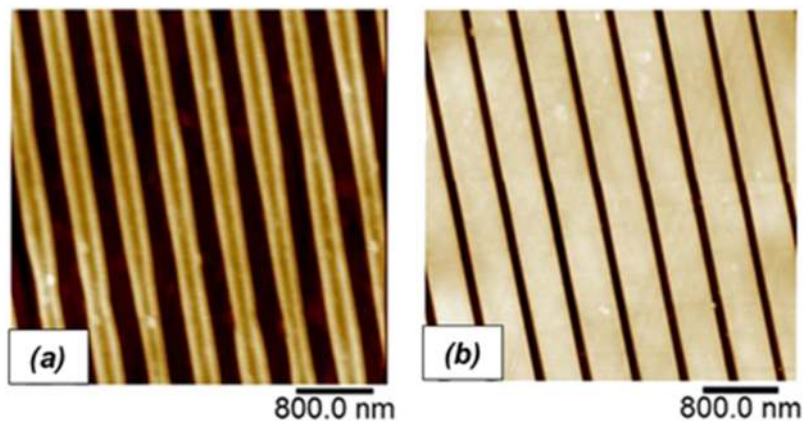


FIG. 2. Atomic force microscopy scans showing the etched relief of the domain structure in the (a) patterned face and (b) opposite polar face.

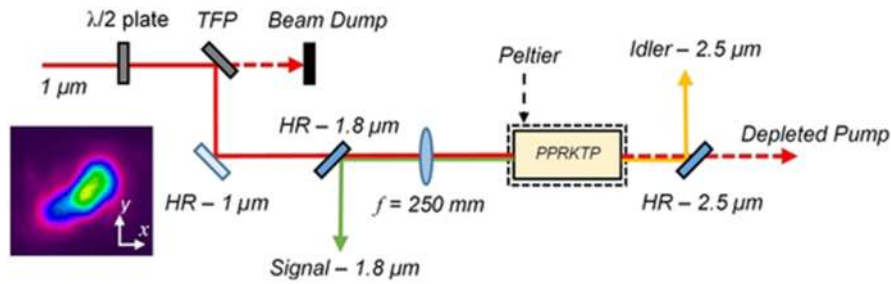


FIG. 3. Experimental layout of the 1.064 μm pumped BWOP with a pump beam profile inset.

Nd:YAG, master-oscillator-power amplifier system operating at 1.064 μm . The pump source had a pulse duration of 13 ns (FWHM) and a repetition rate of 100 Hz with the maximum output energy of 200 mJ.

The amount of pump energy steered toward the MOPO was varied with a half-wave plate and thin-film polarizer combination. The pump beam had an elliptical Gaussian spatial profile with M^2 values of 3.2 and 3.3 in the x and y directions, respectively. It was guided through a CaF_2 mirror which was reflective for the signal wavelength. The pump beam was focused by a spherical CaF_2 lens with a focal length of $f = 250$ mm. The resulting beam radius in the crystal was measured to be $w_{0x} = 298$ μm and $w_{0y} = 297$ μm ($1/e^2$) with the travelling knife-edge method. The crystal was positioned to have its center coincide with the focus of the beam. The crystal was mounted onto a holder with a Peltier element for temperature stabilization. The Peltier temperature was set to room temperature around 21 $^\circ\text{C}$. Finally, a mirror that is highly reflective for the idler wavelength was placed after the crystal to separate the idler from the depleted pump.

The BWOP started oscillation when the pump energy inside the crystal reached 1.5 mJ. This corresponds to the threshold intensity of 83 MW cm^{-2} . This threshold intensity is similar to that typically achieved in usual OPOs employing PPKTP as a gain material.²⁴ From the threshold intensity, we can estimate⁶ that the effective nonlinearity in a 7 mm-long structure was 7.5 pm/V, not far from the maximum value of $2d_{33}/\pi = 9.8$ pm/V.²⁵ This is a good indication of the high quality of the QPM structure considering that the crystal contains approximately 28 000 periodically inverted domains, each nominally being only 250 nm-long. With such low threshold intensity, the BWOP could be readily pumped up to the energy of about 6.5 mJ, before reaching energy fluence of 5 J/cm^2 , which is half the optical damage threshold.¹⁷ The BWOP output energy, efficiency, and pump depletion characteristics are shown in Fig. 4(a). Pumping with a maximum input energy of 6.48 mJ and output energies of 1.96 mJ and 1.46 mJ were reached for the signal and the idler, respectively. At the maximum pump energy, the total conversion of the device was measured to be 53%. Correspondingly, the pump depletion was measured to be 53.8%.

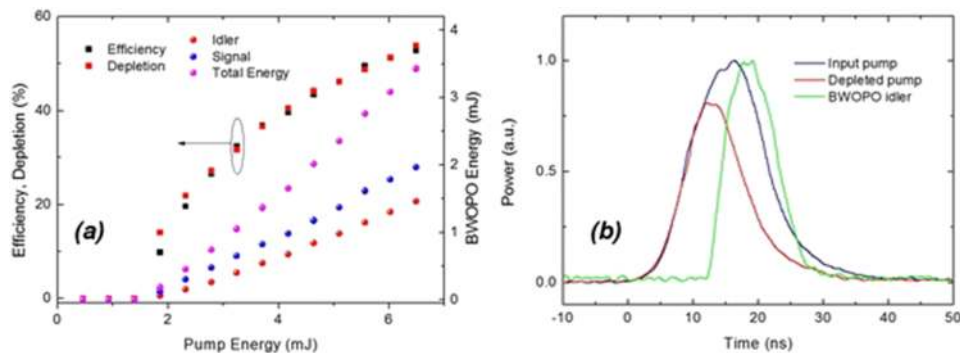


FIG. 4. (a) BWOP efficiency and pump depletion and generated energies as a function of pump energy; efficiency (black squares), depletion (red squares). (b) Normalized temporal traces of the input pump (blue line), depleted pump (red line), and BWOP idler (green line) pulses.

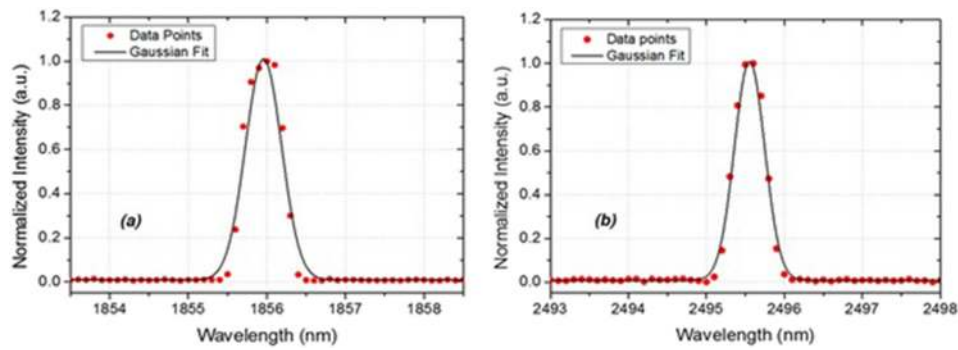


FIG. 5. Spectra of the generated signal (a) and idler (b) from the BWOPO.

The temporal traces of the pump, depleted pump, and the forward-generated BWOPO idler at 2.495 μm , measured at the input pump energy of 6 mJ, are shown in Fig. 4(b). The traces were measured with a 2 GHz analog-bandwidth oscilloscope. For the pump measurement, we employed the Si p-i-n diode with a rise time of 1 ns (Thorlabs), while the idler pulse was measured with the HgCdTe photo-electromagnetic detector (Vigo System) with the rise time below 1 ns. At this pump energy, the FWHM length of the BWOPO pulse is 9 ns. Here the BWOPO is operating 4-times above threshold. However, neither temporal traces nor efficiency graph in Fig. 4(a) shows any signs of back-conversion. In standard OPOs employing co-propagating TWM, back-conversion is usually quite prominent at these pump levels even in singly resonant cavities. In BWOPO, the back-conversion process is strongly limited due to the inherent property of counter-propagating TWM which ensures that the maximum intensities of the signal and idler are reached at the opposite ends of the nonlinear crystal.^{4,5}

Spectra of the BWOPO signal and idler measured with the Jobin-Yvon-Horiba iHR 550 spectrometer are shown in Fig. 5. The center wavelengths of the signal and idler were measured to be approximately 1856 nm and 2495.5 nm, respectively. A Gaussian fit was applied to the measured signal and idler data. From this, the bandwidth (FWHM) of the signal and idler was estimated to be about 0.5 nm. For the spectrometer with the 300 l/mm grating and a 80 μm output slit, this represents the spectrometer-limited linewidth. For the measured BWOPO signal pulse length, the transform-limited spectral width would be 49 MHz. In Fig. 6, we show a comparison of the BWOPO idler spectrum to that measured in a singly resonant OPO employing co-propagating TWM in a

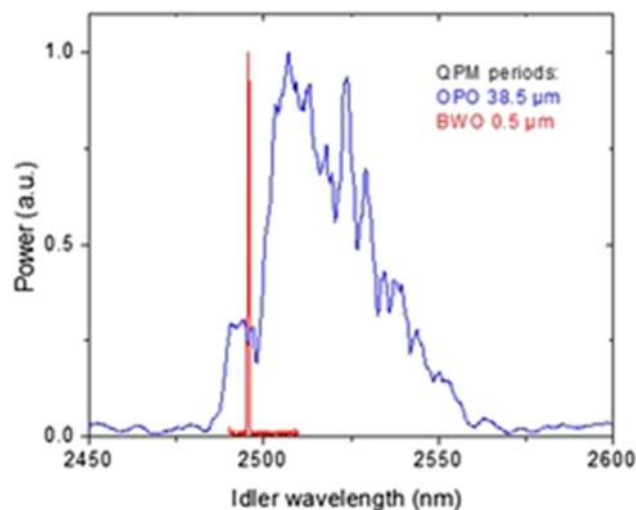


FIG. 6. Normalized idler spectra of the PPRKTP BWOPO (red line) and a singly resonant OPO using 7 mm-long PPRKTP with a period of 38.5 μm (blue line).

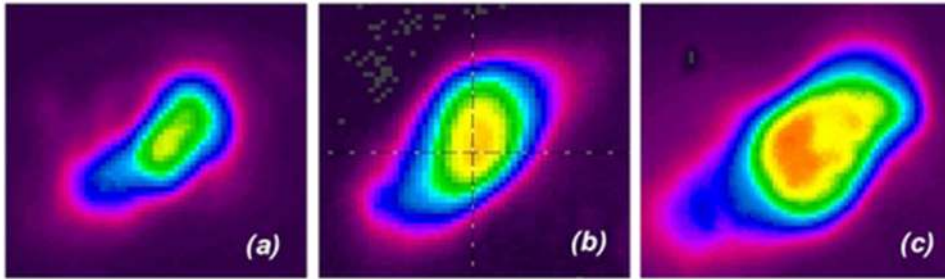


FIG. 7. Far-field beam profiles of the pump (a) and BWPO idler for (b) 2.5 mJ and (c) 6 mJ input pump energy.

7 mm-long PPRKTP with the periodicity of $38.5 \mu\text{m}$. Both devices were pumped with the same laser source. Stark difference in the bandwidth in the OPO and BWPO can be understood considering that for single-frequency pumping the parametric gain bandwidth in co-propagating TWM is inversely proportional to the signal and idler group velocity difference, $\Delta\nu_{OPO} \propto v_{gs}v_{gi}/|v_{gs} - v_{gi}|$.²⁶ In the counter-propagating TWM case, the parametric gain bandwidth is inversely proportional to the sum of the group velocities, $\Delta\nu_{OPO} \propto v_{gs}v_{gi}/(v_{gs} + v_{gi})$.

The spatial intensity profile of the pump and the BWPO beams was measured with the aid of a pyroelectric camera (Pyrocam III). In Fig. 7, we show the far field spatial profiles of the pump and the idler at two different pump energies. Cut-on filters were used when measuring idler and signal beams in order to prevent any residual pump light exposure. The idler beam profile was similar to that of the input pump. In general, several factors can affect the spatial intensity distribution in parametric devices, e.g., intensity distribution of the pump, its spatial phase distribution, back-conversion processes, spatial pump depletion, and homogeneity of the QPM structure. However, in our case, considering that our injection seeded pump gives a beam with relatively high spatial coherence, that the QPM structure was homogeneous, and the virtual absence of back-conversion processes, the BWPO spatial beam profile should be mainly determined by the pump intensity distribution and the spatial pump depletion. This is also the case for the signal beam profile, which showed a similar structure to that of the pump beam.

IV. CONCLUSION

In conclusion, in this work, we demonstrated a BWPO with PPRKTP where the higher-frequency wave, the signal, is generated in the direction opposite to that of the pump. BWPO with backward signal generation is beneficial if cascaded parametric oscillation processes need to be avoided. For pumping at $1.064 \mu\text{m}$, achieving such an oscillation regime required QPM periodicities shorter than 600 nm . The PPRKTP structure with a periodicity of 509 nm and the length of 7 mm showed an effective nonlinearity of 7.4 pm/V , which allowed reaching BWPO oscillation threshold comparable to those typically achieved in co-propagating OPOs using the PPRKTP nonlinear crystals. Such low thresholds in turn give the opportunity to pump BWPO with injection-seeded Q-switched Nd:YAG laser sources for generation of transform-limited pulses in the near and mid-infrared. Due to low threshold, the BWPO could reach an efficiency exceeding 53% for the pump energy fluence half the optical damage threshold. Counter-propagating TWM in BWPO strongly suppresses back-conversion and multi-step $\chi^{(2)}$: $\chi^{(2)}$ processes, therefore preventing spectral broadening and deterioration of the spatial beam distribution and higher conversion efficiencies. With a total output of 3.42 mJ and a simple configuration, the BWPO can be used for seeding narrowband high-energy optical parametric amplifiers, e.g., in differential absorption LIDARs. It should be noted that precise tunability over the range of hundreds of GHz can readily be achieved in the BWPO¹⁰ by simple angular rotation of the crystal.

ACKNOWLEDGMENTS

The authors would like to acknowledge VR and the Swedish Foundation for Strategic Research for generous funding.

- ¹ S. E. Harris, *Appl. Phys. Lett.* **9**, 114–116 (1966).
- ² R. Kompfner and N. T. Williams, *Proc. IRE* **41**, 1602–1611 (1953).
- ³ H. Heffner, *Proc. IRE* **42**, 930–937 (1954).
- ⁴ Y. J. Ding and J. B. Khurgin, *IEEE J. Quantum Electron.* **32**, 1574–1582 (1996).
- ⁵ Y. J. Ding and J. B. Khurgin, *J. Nonlinear Opt. Phys. Mater.* **5**, 223–246 (1996).
- ⁶ H. Su, S.-C. Ruan, and Y. Guo, *J. Opt. Soc. Am. B* **23**, 1626–1629 (2006).
- ⁷ C. Canalias and V. Pasiskevicius, *Nat. Photonics* **1**, 459–462 (2007).
- ⁸ G. Strömqvist, V. Pasiskevicius, C. Canalias, and C. Montes, *Phys. Rev. A* **84**, 023825 (2011).
- ⁹ C. Montes, B. Gay-Para, M. De Micheli, and P. Aschieri, *J. Opt. Soc. Am. B* **31**(12), 3186–3192 (2014).
- ¹⁰ G. Strömqvist, V. Pasiskevicius, and C. Canalias, *Appl. Phys. Lett.* **98**, 051108 (2011).
- ¹¹ C. Chuu and S. E. Harris, *Phys. Rev. A* **83**, 061803R (2011).
- ¹² A. Amediek, A. Fix, M. Wirth, and G. Ehret, *Appl. Phys. B* **92**, 295–302 (2008).
- ¹³ A. Berrou, M. Raybaut, A. Godard, and M. Lefebvre, *Appl. Phys. B* **98**, 217–230 (2010).
- ¹⁴ B. Hardy, A. Berrou, S. Guilbaud, M. Raybaut, and M. Lefebvre, *Opt. Lett.* **36**, 678–680 (2011).
- ¹⁵ M. M. Fejer, G. A. Magel, D. H. Jundt, and R. L. Byer, *IEEE J. Quantum Electron.* **28**, 2631–2654 (1992).
- ¹⁶ A. Hildenbrand, F. R. Wagner, H. Akhouayri, J.-Y. Natoli, M. Commandré, F. Théodore, and H. Albrecht, *Appl. Opt.* **48**(21), 4263 (2009).
- ¹⁷ R. S. Coetzee, N. Thilman, A. Zukauskas, C. Canalias, and V. Pasiskevicius, *Opt. Mater. Express* **5**, 2090–2095 (2015).
- ¹⁸ K. Fradkin, A. Arie, A. Skliar, and G. Rosenman, *Appl. Phys. Lett.* **74**, 914–916 (1999).
- ¹⁹ A. Zukauskas, A.-L. Viotti, C. Liljestränd, V. Pasiskevicius, and C. Canalias, *Sci. Rep.* **7**, 8037 (2017).
- ²⁰ Q. Jiang, P. A. Thomas, K. B. Hutton, and R. C. C. Ward, *J. Appl. Phys.* **92**, 2717–2723 (2002).
- ²¹ S. Tjörnhammar, V. Maestroni, A. Zukauskas, T. K. Uždavinyš, C. Canalias, F. Laurell, and V. Pasiskevicius, *Opt. Mater. Express* **5**, 2951 (2015).
- ²² C. Liljestränd, A. Zukauskas, V. Pasiskevicius, and C. Canalias, *Opt. Lett.* **42**(13), 2435–2438 (2017).
- ²³ A. Zukauskas, G. Strömqvist, V. Pasiskevicius, F. Laurell, M. Fokine, and C. Canalias, *Opt. Mater. Express* **1**, 1319–1325 (2011).
- ²⁴ J. Hellström, V. Pasiskevicius, H. Karlsson, and F. Laurell, *Opt. Lett.* **25**, 174 (2000).
- ²⁵ M. V. Pack, D. J. Armstrong, and A. V. Smith, *Appl. Opt.* **43**, 3319 (2004).
- ²⁶ C. Manzoni and G. Cerullo, *J. Opt.* **18**, 103501 (2016).